Brief Report

DOI: 10.5582/bst.2018.01218

Purification, crystallization and preliminary X-ray crystallographic studies on the C-terminal domain of the flagellar protein FliL from *Helicobacter pylori*

Kar Lok Chan[1], Mayra A. Machuca[1], Mohammad Mizanur Rahman[1], Mohammad Firoz Khan[1], Daniel Andrews[1], Anna Roujeinikova[1,2,*]

[1] *Infection and Immunity Program, Monash Biomedicine Discovery Institute, Department of Microbiology, Monash University, Clayton, Victoria, Australia;*
[2] *Department of Biochemistry and Molecular Biology, Monash University, Clayton, Victoria, Australia.*

Summary **FliL is an inner membrane protein, occupying a position between the rotor and the stator of the bacterial flagellar motor. Its proximity to, and interactions with, the MS (membrane and supramembranous) ring, the switch complex and the stator proteins MotA/B suggests a role in recruitment and/or stabilization of the stator around the rotor, although the precise role of FliL in the flagellum remains to be established. In this study, recombinant C-terminal domain of *Helicobacter pylori* FliL (amino-acid residues 81-183) has been expressed in *Escherichia coli* and purified to > 98% homogeneity. Purified recombinant protein behaved as a monomer in solution. Crystals were obtained by the hanging-drop vapour-diffusion method using ammonium phosphate monobasic as a precipitant. These crystals belong to space group *P*1, with unit-cell parameters *a* = 62.5, *b* = 82.6, *c* = 97.8 Å, *α* = 67.7, *β* = 83.4, *γ* = 72.8°. A complete data set has been collected to 2.8 Å resolution using synchrotron radiation. This is an important step towards elucidation of the function of FliL in the bacterial flagellar motor.**

Keywords: Flagellar motor, Helicobacter pylori, protein crystallization, X-ray crystallography

1. Introduction

Helicobacter pylori infection of the human stomach is associated with chronic gastritis and gastric ulcers and has a strong correlation with gastric cancer (*1-4*). Motility by means of a tuft of sheathed, unipolar flagella is an essential colonization factor (*5,6*). The flagellum has two major components, the cell wall-embedded basal body, that spans both inner and outer membrane, and the extracellular filament composed of flagellins (*7*). The basal body consists of the cytoplasmic C-ring, the MS (membrane and supramembranous) ring, the rod, the export apparatus and the stator. The basal body serves as a rotary motor that spins the filament, with the energy for rotation derived from the proton-motive force (*8*). Rotation is driven by the interaction of the C-ring with several circumferentially positioned stator complexes, composed of the cytoplasmic protein MotA and peptidoglycan-anchored MotB (*7,9,10*).

Whilst it is well understood that MotA/MotB complex functions as a proton channel that does bind efficiently to the cell wall and is 'plugged' until it incorporates into the motor (*11-14*), little is known about the mechanism by which the stator assembles around the rotor and switches into a proton-conducting state. Previous studies of the flagellar motor in *Salmonella* and *E. coli* suggested that conserved protein FliL, which contains a single transmembrane helix and an approximately 150 a.a. long periplasmic domain, plays an important role in the stator assembly, as it has been shown to interact with the stator proteins MotA and MotB, as well as the rotor components FliF (MS ring) and FliG (C ring) (*15*). Deletion of *Salmonella fliL* caused only a small reduction in swimming, but eliminated swarming (*16*). It is thought that FliL is required for *Salmonella* swarming, when the motor

**Address correspondence to:*
Dr. Anna Roujeinikova, Infection and Immunity Program, Monash Biomedicine Discovery Institute Department of Microbiology, Department of Biochemistry and Molecular Biology, Monash University, Clayton, Victoria, Australia.
E-mail: anna.roujeinikova@monash.edu

must produce sufficient torque to move through viscous mediums (high load), because it enhances the interaction between MotA and MotB, increases the time that the stator is engaged with the rotor and/or improves the efficiency of proton flow through the motor (*15*). In addition, it has been suggested that FliL may assist the release of the MotB plug helices from the membrane and thus activate the stator complexes upon their assembly into the motor, as point mutations within the plug suppressed the motility defect of the *Salmonella* Δ*fliL* mutant (*15*).

The deletion of the *fliL* gene in *Rhodobacter sphaeroides* impaired its motility (*17*). It has been proposed that in *R. sphaeroides*, FliL, together with MotF, promotes the opening of the proton channel through FlgT, which interacts with MotB and triggers the release of the plug (*18-20*). Similarly, a *fliL* mutant of *Caulobacter crescentus* had non-functional flagella, indicating the essential role of FliL in flagellar rotation (*21*). FliL defect in *Proteus mirabilis* resulted in the impairment of motility and the synthesis of flagellin proteins, and it has been suggested that *P. mirabilis* FliL may also serve as a surface sensor that regulates the gene expression (*22-24*).

In *Borrelia burgdorferi*, the deletion of FliL altered the periplasmic flagellar orientation and caused motility impairment (*25*). Crucially, cryo-electron tomography of the *B. burgdorferi* flagellar motor revealed that FliL is located between the rotor and the stator (*25*), a position consistent with the hypothetical role of FliL in the assembly and/or stabilization of the stator around the rotor. Similarly, in the recent cryo-electron tomography study of the *H. pylori* flagellar motor, the putative FliL ring is clearly seen between the MS ring and the stator, although the role of FliL in the motor function in *H. pylori* remains to be established (*26*).

FliL shares no significant sequence similarity to any protein of a known structure. However, it is anticipated that determination of the crystal structure of its soluble periplasmic domain will provide a critical insight into its function through identification of functional homologues with a similar fold, as protein structure is more conserved than sequence. The production of the crystals of the periplasmic domain of FliL from *Vibrio alginolyticus* was reported (*27*), but no structure is available yet. Here, we report the cloning, purification, crystallization and the preliminary X-ray crystallographic analysis of the C-terminal periplasmic domain of *H. pylori* FliL.

2. Materials and Methods

2.1. *Gene cloning and overexpression*

The membrane topology and disordered regions of FliL from *H. pylori* strain SS1 (Genbank ID AQM65563.1) were predicted by using the TOPCONS (*http://topcons.net/*) (*28*) and DISOPRED3 (*http://bioinf.cs.ucl.ac.uk/disopred*) (*29*) servers, respectively (Figure 1). The coding sequence for the C-terminal domain of FliL (FliL-C, comprising amino-acid residues 81-183) was codon optimized for expression in *Escherichia coli*, synthesized and ligated into the pET151/D-TOPO vector (Invitrogen, Waltham, MA, USA) by GenScript (Piscataway, NJ, USA) to produce an expression vector that harbors an N-terminal His_6 tag followed by a tobacco etch virus (TEV) protease cleavage site. The 109-residue recombinant protein used for crystallization comprised residues 81-183 of FliL plus six additional residues from the TEV cleavage site (GIDPFT).

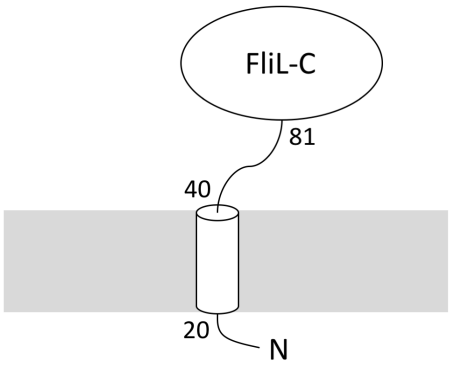

Figure 1. The predicted membrane topology of *H. pylori* FliL and the boundaries of the periplasmic domain CtaB FliL-C characterized in this study.

Escherichia coli strain BL21(DE3)-RIPL cells (Stratagene, La Jolla, CA, USA) were transformed with the expression vector and cultured at 37°C in LB medium containing 50 mg/L ampicillin. Overexpression of FliL-C was induced with 1 mM isopropyl-D-1-thiogalactopyranoside at an OD_{600} of 0.6. The cells were grown for a further 4 h at 37°C and then harvested by centrifugation at 4,800 g for 15 min at 4°C.

2.2. *Purification and determination of the oligomeric state*

Protein was purified by following the procedure based on that described in (*30*). Briefly, the cell pellet was resuspended in buffer A (20 mM Tris-HCl pH 8.0, 150 mM NaCl, 1 mM phenylmethanesulfonyl fluoride) and lyzed using an Avestin EmulsiFlex-C5 high-pressure homogenizer (Avestin, Ottawa, Canada). Cell debris was removed by centrifugation at 10,000 g for 20 min (4°C). NaCl and imidazole were then added to the supernatant to final concentrations of 500 and 10 mM, respectively, after which the supernatant was loaded onto a 5 mL Ni-NTA affinity column (GE Healthcare, Chicago, IL, USA) pre-equilibrated in buffer B (20 mM Tris-HCl pH 8.0, 500 mM NaCl, 20 mM imidazole), washed with 10 column volumes of the same buffer and eluted with buffer C (20 mM Tris-HCl pH 8.0, 500 mM NaCl, 500 mM imidazole). The hexahistidine tag was cleaved off using TEV protease (Invitrogen, Waltham, MA, USA) while dialyzing the sample against buffer

D [20 mM Tris-HCl pH 8.0, 150 mM NaCl, 2 mM dithiothreitol, 1% (v/v) glycerol] at 10°C overnight. NaCl and imidazole were then added to the sample to final concentrations of 500 and 20 mM, respectively, and the TEV protease and the uncleaved protein were removed by passing the sample through the Ni-NTA column. The flowthrough was concentrated to 2 mL in a VivaSpin 10,000 Da cutoff concentrator and passed through a Superdex 200 HiLoad 26/60 gel-filtration column (GE Healthcare) equilibrated with buffer E (10 mM Tris-HCl pH 8.0, 150 mM NaCl). Protein concentration was determined using the Bradford assay (*31*), and protein purity was evaluated using SDS-PAGE. The oligomeric state of FliL-C in solution was determined by calculating the molecular weight (MW) using a calibration plot of log MW versus the retention volume [$V_{retention}$ (mL) = 549.3 – 73.9 × log MW] (*32*).

2.3. *Protein buffer optimization*

Thermal shift analysis of protein stability in different buffers was performed using a Rotor-Gene Q Real-time PCR instrument (QIAGEN, Hilden, Germany). FliL-C was concentrated to 1.0 mM in buffer E and then diluted 100 fold with a series of test buffers containing 10×SYPRO Orange reagent (purchased from Sigma-Aldrich, St. Louis, MO, USA as 5000× stock, catalogue number S5692) in a final volume of 25 µL. The samples were thermally denatured by heating them from 35°C to 90°C at a ramp rate of 0.5°C/min. Protein denaturation was monitored by following SYPRO Orange fluorescence emission (λ_{ex} 530 nm/λ_{em} 555 nm). The denaturation data were fit to a derivation of the Boltzmann equation for the two-state unfolding model to obtain the midpoint of denaturation (the melting temperature T_m) (*33*). All experiments were performed in triplicates.

2.4. *Crystallization*

FliL-C was concentrated to 8 mg/ml and centrifuged for 20 min at 13,000 g to clarify the solution. The crystallization screening was carried out by the hanging-drop vapour-diffusion method using an automated Phoenix crystallization robot (Art Robbins Instruments, Sunnyvale, CA, USA) and commercial screens JBS Classic HTS1, JBS Classic HTS2, JBS JCSG++ (Jena Bioscience, Jena, Germany), Crystal Screen HT, and PEG/Ion HT (Hampton Research, Laguna Niguel, CA). The crystallization droplets comprised 100 nL protein solution mixed with 100 nL reservoir solution, and were equilibrated against 50 µL reservoir solution in a 96-well Art Robbins CrystalMation Intelli-Plate (Hampton Research). Clusters of needle-like crystals appeared after one day in condition G5 of the JBS Classic HTS2 screen, which contained 0.5 M ammonium di-hydrogen phosphate and 0.2 M trisodium citrate, and in condition A11, which contained 1.0 M ammonium phosphate monobasic and 0.1 M trisodium citrate dehydrate pH 5.6. Optimization of the condition to improve the crystal quality yielded thin plate-like crystals using 0.4 M ammonium phosphate monobasic and 0.1 M trisodium citrate dehydrate pH 5.6 and a protein concentration of 12 mg/mL. These crystals had maximum dimensions of 0.1 × 0.03 × 0.02 mm.

2.5. *Data collection and processing*

Prior to data collection, the FliL-C crystals were briefly soaked in a cryoprotectant solution (0.48 M ammonium phosphate monobasic, 0.12 M trisodium citrate dehydrate pH 5.6, 20% (v/v) glycerol), and then flash-frozen by plunging in liquid nitrogen. A complete X-ray diffraction data set was collected to 2.8 Å from a single cryo-cooled crystal on the MX1 beamline of the Australian Synchrotron. A total of 360 images were collected using a 0.5° oscillation. The data were processed and scaled using XDS (*34*) and *AIMLESS* from the Collaborative Computational Project, Number 4 (*CCP4*) suite (*35*). Data collection and processing statistics are summarized in Table 1. Calculation of the self- rotation function was performed using the *POLARRFN* program (*35*).

3. Results and Discussion

H. pylori FliL (183 a.a.) was predicted to contain one N-terminal transmembrane (TM) helix (amino-acid residues 20-40), with the protein's amino-terminus in the cytoplasm, followed by a disordered linker region (residues 41-85) connecting the TM helix to the periplasmic domain (Figure 1). For the purpose of protein production for crystallization, the domain boundaries of the recombinant periplasmic domain FliL-C have

Table 1. Data collection and processing. Values in parentheses correspond to the highest resolution shell

Diffraction source	MX1 beamline, Australian Synchrotron
Wavelength (Å)	0.95
Temperature (K)	100
Detector	ADSC Quantum 210r CCD
Rotation per image (º)	0.5
Total rotation range (º)	180
Space group	*P*1
a, b, c (Å)	62.5, 82.6, 97.8
α, β, γ (º)	67.7, 83.4, 72.8
Mosaicity (º)	0.6
Resolution range (Å)	54.16-2.80 (2.91-2.80)
Total No. of reflections	81,483 (9,191)
No. of unique reflections	41,760 (4,676)
Completeness (%)	98.1 (97.6)
Multiplicity	2.0
$\langle I/\sigma(I)\rangle$	5.2 (1.6)
$CC_{1/2}$ (%)	98.5 (71.3)
R_{merge}	0.103 (0.323)
Overall *B* factor from Wilson plot (Å^2)	30.7

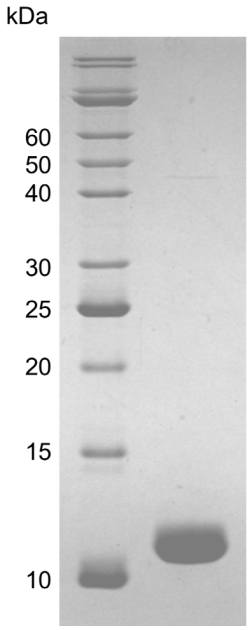

Figure 2. Coomassie Blue-stained 16.5% SDS–PAGE gel of recombinant FliL-C.

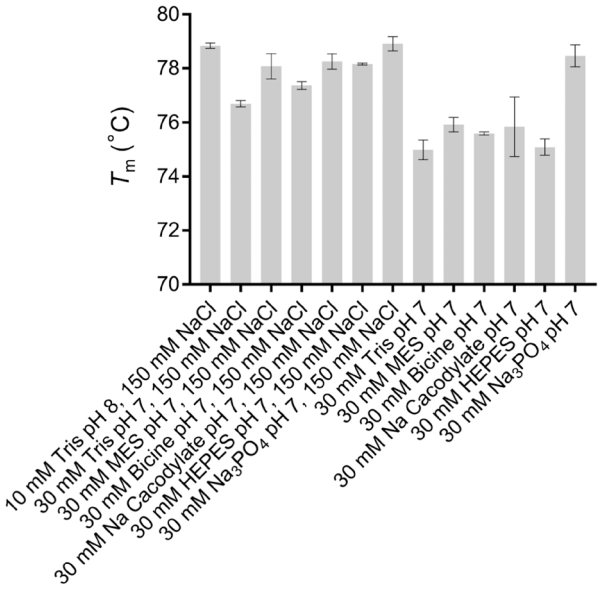

Figure 3. Comparison of the melting temperature T_m of the 10 μM solution of FliL-C in different buffers. Results are means ± S.D. for three independent replicates.

been set at residues 81-183. FliL-C was over-expressed in BL21(DE3)-RIPL cells from the pET151/D-TOPO plasmid, upon induction of T7 polymerase, and purified to > 98% electrophoretic homogeneity based on Coomassie Blue staining of the SDS-PAGE gel (Figure 2). It migrated on SDS-PAGE with an apparent molecular weight of ~12 kDa, which is close to the value calculated from the amino-acid sequence (12.18 kDa).

When subjected to gel filtration, the protein eluted as a single symmetrical peak (data not shown). The particle weight value estimated from the mobility of the gel-filtration column calibrated using globular proteins of a known mass gave the value of approximately 11.2 kDa, which suggested that *H. pylori* FliL-C is monomeric in solution under the tested conditions. This result is in agreement with the previous report on the periplasmic domain of *Vibrio alginolyticus* FliL, which is also primarily monomeric in solution in the concentration range used in this study (*27*).

In preparation for crystallization experiments, we have assessed the protein stability in different buffers using a thermal shift assay (Figure 3), and ascertained that gel-filtration buffer E (10 mM Tris-HCl pH 8.0, 150 mM NaCl) was optimal, as the melting temperature in this buffer was one of the highest among all tested conditions. Thus, no buffer exchange step was needed between gel filtration and crystallization. Crystals of FliL-C were obtained using a sparse-matrix crystallization approach. A complete X-ray diffraction data set was collected for a cryo-cooled crystal of FliL-C (Figure 4) to 2.8 Å using the Australian Synchrotron facility. Autoindexing of the diffraction data using *XDS* was consistent with space group *P*1, with unit-cell parameters $a = 62.5$, $b = 82.6$, $c = 97.8$ Å, $\alpha = 67.7$, $\beta = 83.4$, $\gamma = 72.8°$. The average $I/\sigma(I)$ value

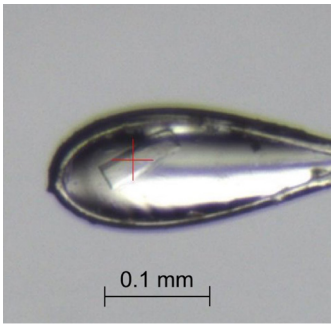

Figure 4. The FliL-C crystal mounted in the cryo-loop prior to data collection at the MX1 station of the Australian Synchrotron.

was 5.2 for all reflections (resolution range 54.2-2.8 Å) and 1.6 in the highest resolution shell (2.91-2.80 Å). Data processing gave an R_{merge} of 0.103 for intensities (0.323 in the highest resolution shell), and these data were 98% complete (98% completeness in the outer shell).

Estimation of the Matthews coefficient V_M (*36*) gave plausible values for 8 ($V_M = 4.6$ Å^3/Da) to 18 ($V_M = 2.1$ Å^3/Da) protein molecules in the asymmetric unit. The $\chi = 90$, $\chi = 120$ and $\chi = 180°$ sections of the self-rotation function were unremarkable. Thus, we are currently not able to establish the protein content of the asymmetric unit. A search for heavy-atom derivatives with the aim to solve the structure using multiple isomorphous replacement and/or multi-wavelength anomalous dispersion methods is underway. Production of the recombinant periplasmic domain of *H. pylori* FliL in its pure form will enable proteomics-based identification of its interacting partners in the flagellar motor. Furthermore, generation of well-ordered, reproducible crystals will allow determination of its 3-D

structure which would be an important step towards our understanding of its function in the bacterial flagellum.

Acknowledgements

Part of this research was undertaken on the MX1 beamline of the Australian Synchrotron, Victoria, Australia. We thank the AS staff for their assistance with data collection. We are also grateful to Dr. Danuta Maksel and Dr. Geoffrey Kong at the Monash Macromolecular Crystallisation Facility for assistance with the robotic crystallization trials. Mayra A. Machuca was a recipient of a PhD scholarship from the Departamento Admistrativo de Ciencia, Tecnología e Innovación COLCIENCIAS.

References

1. Warren JR, Marshall BJ. Unidentified curved bacilli on gastric epithelium in active chronic gastritis. Lancet. 1983; 1:1273-1275.
2. Watanabe T, Tada M, Nagi H, Sasaki S, Nakao M. *Helicobacter pylori* infection induces gastric cancer in Mongolian gerbils. Gastroenterology. 1998; 115:642-648.
3. Honda S, Fujioka T, Tokieda M, Satoh R, Nishizono A, Nasu M. Development of *Helicobacter pylori*-induced gastric carcinoma in mongolian gerbils. Cancer Res. 1998; 58:4255-4259.
4. Forman D, Coleman M, Debacker G, *et al*. An international association between *Helicobacter pylori* infection and gastric cancer. Lancet. 1993; 341:1359-1362.
5. Eaton KA, Morgan DR, Krakowka S. Motility as a factor in the colonisation of gnotobiotic piglets by *Helicobacter pylori*. J Med Microbiol. 1992; 37:123-127.
6. Geis G, Suerbaum S, Forsthoff B, Leying H, Opferkuch W. Ultrastructure and biochemical studies of the flagellar sheath of *Helicobacter pylori*. J Med Microbiol. 1993; 38:371-377.
7. Terashima H, Kojima S, Homma, M. Chapter 2: Flagellar Motility in Bacteria. Structure and Function of Flagellar Motor. In: International Review of Cell and Molecular Biology, Vol. 270, 2008; pp. 39-85.
8. Manson MD, Tedesco P, Berg HC, Harold FM, Van der Drift C. A protonmotive force drives bacterial flagella. Proc Natl Acad Sci U S A. 1977; 74:3060-3064.
9. Roujeinikova A. Crystal structure of the cell wall anchor domain of MotB, a stator component of the bacterial flagellar motor: Implications for peptidoglycan recognition. Proc Natl Acad Sci U S A. 2008; 105:10348-10353.
10. Reboul CF, Andrews DA, Nahar MF, Buckle AM, Roujeinikova, A. Crystallographic and molecular dynamics analysis of loop motions unmasking the peptidoglycan-binding site in stator protein MotB of flagellar motor. PLoS one. 2011; 6:e18981.
11. O'Neill J, Xie M, Hijnen M, Roujeinikova A. Role of the MotB linker in the assembly and activation of the bacterial flagellar motor. Acta Crystallogr D Biol Crystallogr. 2011; 67:1009-1016.
12. Andrews DA, Nesmelov YE, Wilce MC, Roujeinikova A. Structural analysis of variant of *Helicobacter pylori* MotB in its activated form, engineered as chimera of MotB and leucine zipper. Sci Rep. 2017; 7:13435.
13. Wilson ML, Macnab RM. Co-overproduction and localization of the *Escherichia coli* motility proteins motA and motB. J Bacteriol. 1990; 172:3932-3939.
14. Hosking ER, Vogt C, Bakker EP, Manson MD. The *Escherichia coli* MotAB proton channel unplugged. J Mol Biol. 2006; 364:921-937.
15. Partridge JD, Nieto V, Harshey RM. A new player at the flagellar motor: FliL controls both motor output and bias. MBio. 2015; 6:e02367.
16. Attmannspacher U, Scharf BE, Harshey RM. FliL is essential for swarming: motor rotation in absence of FliL fractures the flagellar rod in swarmer cells of *Salmonella enterica*. Mol Microbiol. 2008; 68:328-341.
17. Suaste-Olmos F, Domenzain C, Mireles-Rodríguez JC, Poggio S, Osorio A, Dreyfus G, Camarena L. The flagellar protein FliL is essential for swimming in *Rhodobacter sphaeroides*. J Bacteriol. 2010; 192:6230-6239.
18. Fabela S, Domenzain C, De la Mora J, Osorio A, Ramirez-Cabrera V, Poggio S, Dreyfus G, Camarena L. A distant homologue of the FlgT protein interacts with MotB and FliL and is essential for flagellar rotation in *Rhodobacter sphaeroides*. J Bacteriol. 2013; 195:5285-5296.
19. Suaste-Olmos F, Domenzain C, Mireles-Rodríguez JC, Poggio S, Osorio A, Dreyfus G, Camarena L. The flagellar protein FliL is essential for swimming in *Rhodobacter sphaeroides*. J Bacteriol. 2010; 192:6230-6239.
20. Ramírez-Cabrera V1, Poggio S, Domenzain C, Osorio A, Dreyfus G, Camarena L. A novel component of the *Rhodobacter sphaeroides* Fla1 flagellum is essential for motor rotation. J Bacteriol. 2012; 194:6174-6183.
21. Jenal U, White J, Shapiro L. *Caulobacter* flagellar function, but not assembly, requires FliL, a non-polarly localized membrane protein present in all cell types. J Mol Biol. 1994; 243:227-244.
22. Cusick K, Lee YY, Youchak B, Belas R. Perturbation of FliL interferes with *Proteus mirabilis* swarmer cell gene expression and differentiation. J Bacteriol. 2012; 194:437-447.
23. Lee YY, Patellis J, Belas R. Activity of *Proteus mirabilis* FliL is viscosity dependent and requires extragenic DNA. J Bacteriol. 2013; 195:823-832.
24. Lee YY, Belas R. Loss of FliL alters *Proteus mirabilis* surface sensing and temperature-dependent swarming. J Bacteriol. 2015; 197:159-173.
25. Motaleb MA, Pitzer JE, Sultan SZ, Liu J. A novel gene inactivation system reveals altered periplasmic flagellar orientation in a *Borrelia burgdorferi fliL* mutant. J Bacteriol. 2011; 193:3324-3331.
26. Qin Z, Lin W, Zhu S, Franco AT, Liu J. Imaging the motility and chemotaxis machineries in *Helicobacter pylori* by cryo-electron tomography. J Bacteriol. 2017; 199:e00695-16.
27. Kumar A, Isumi M, Sakuma M, Zhu S, Nishino Y, Onoue Y, Kojima S, Miyanoiri Y, Imada K, Homma M. Biochemical characterization of the flagellar stator-associated inner membrane protein FliL from *Vibrioalginolyticus*. J Biochem. 2017; 161:331-337.
28. Tsirigos KD, Peters C, Shu N, Kall L, Elofsson A. The TOPCONS web server for consensus prediction of

membrane protein topology and signal peptides. Nucleic Acids Res. 2015; 43:W401-407.
29. Jones DT, Cozzetto D. DISOPRED3: precise disordered region predictions with annotated protein-binding activity. Bioinformatics. 2015; 31:857-863.
30. Woon AP, Tohidpour A, Alonso H, Saijo-Hamano Y, Kwok T, Roujeinikova A. Conformational analysis of isolated domains of *Helicobacter pylori* CagA. PLoS one. 2013; 8:e79367.
31. Bradford MM. A rapid and sensitive for the quantitation of microgram quantitites of protein utilizing the principle of protein-dye binding. Anal Biochem. 1976; 72:248-254.
32. Modak JK, Revitt-Mills SA, Roujeinikova A. Cloning, purification and preliminary crystallographic analysis of the complex of *Helicobacter pylori* α-carbonic anhydrase with acetazolamide. Acta Crystallogr Sect F Struct Biol Cryst Commun. 2013; 69:1252-1255.
33. Orwig SD, Lieberman RL. Biophysical characterization of the olfactomedin domain of myocilin, an extracellular matrix protein implicated in inherited forms of glaucoma. PLoS one. 2011; 6:e16347.
34. Kabsch W. XDS. Acta Crystallogr D Biol Crystallogr. 2010; 66:125-132.
35. Winn MD, Ballard CC, Cowtan KD, Dodson EJ, Emsley P, Evans PR, Keegan RM, Krissinel EB, Leslie AG, McCoy A. Overview of the CCP4 suite and current developments. Acta Crystallogr D Biol Crystallogr. 2011; 67:235-242.
36. Matthews BW. Solvent content of protein crystals. J Mol Biol. 1968; 33:491-497.

(Received September 11, 2018; Revised December 10, 2018; Accepted December 21, 2018)